



Cite this: *Phys. Chem. Chem. Phys.*,  
2015, 17, 25297

# Effect of H bond removal and changes in the position of the iron–sulphur head domain on the spin–lattice relaxation properties of the $[2\text{Fe}–2\text{S}]^{2+}$ Rieske cluster in cytochrome $bc_1$ †

Marcin Sarewicz, Małgorzata Dutka, Rafał Pietras, Arkadiusz Borek and Artur Osyczka\*

Here, comparative electron spin–lattice relaxation studies of the  $2\text{Fe}–2\text{S}$  iron–sulphur (Fe–S) cluster embedded in a large membrane protein complex – cytochrome  $bc_1$  – are reported. Structural modifications of the local environment alone (mutations S158A and Y160W removing specific H bonds between Fe–S and amino acid side chains) or in combination with changes in global protein conformation (mutations/inhibitors changing the position of the Fe–S binding domain within the protein complex) resulted in different redox potentials as well as  $g$ -,  $g$ -strain and the relaxation rates ( $T_1^{-1}$ ) for the Fe–S cluster. The relaxation rates for  $T < 25$  K were measured directly by inversion recovery, while for  $T > 60$  K they were deduced from simulation of continuous wave EPR spectra of the cluster using a model that included anisotropy of Lorentzian broadening. In all cases, the relaxation rate involved contributions from direct, second-order Raman and Orbach processes, each dominating over different temperature ranges. The analysis of  $T_1^{-1}(T)$  over the range 5–120 K yielded the values of the Orbach energy ( $E_{\text{Orb}}$ ), Debye temperature  $\theta_D$  and Raman process efficiency  $C_{\text{Ram}}$  for each variant of the protein. As the Orbach energy was generally higher for mutants S158A and Y160W, compared to wild-type protein (WT), it is suggested that H bond removal influences the geometry leading to increased strength of antiferromagnetic coupling between two Fe ions of the cluster. While  $\theta_D$  was similar for all variants ( $\sim 107$  K), the efficiency of the Raman process generally depends on the spin–orbit coupling that is lower for S158A and Y160W mutants, when compared to the WT. However, in several cases  $C_{\text{Ram}}$  did not only correlate with spin–orbit coupling but was also influenced by other factors – possibly the modification of protein rigidity and therefore the vibrational modes around the Fe–S cluster that change upon the movement of the iron–sulphur head domain.

Received 15th May 2015,  
Accepted 25th August 2015

DOI: 10.1039/c5cp02815a

www.rsc.org/pccp

## Introduction

Iron–sulphur proteins are common elements of many bioenergetic systems in which they play the role of electron carriers or constitute catalytic sites of enzymes involved in energy conversion.<sup>1</sup> The active sites of these proteins bind a compact inorganic cluster that usually contains two, three or four iron

ions bridged by sulphur ions.<sup>2,3</sup> These clusters are chelated by proteins through either cysteine or, in the case of Rieske clusters, by cysteine and histidine side chains. A characteristic feature of the iron–sulphur clusters is the presence of strong antiferromagnetic coupling between high-spin iron ions that, depending on the redox state, leads to the formation of the diamagnetic ( $S = 0$ ) or paramagnetic state ( $S = 1/2$ ) in the centre with average  $g$ -tensor values lower than  $g_e = 2.0023$ .<sup>4,5</sup> Electron paramagnetic resonance spectroscopy (EPR) is widely recognised as the main experimental tool to investigate the properties of paramagnetic iron–sulphur proteins.<sup>2,6</sup>

The family of 2-iron-2-sulphur proteins is divided into two classes according to the average value of  $g$ -tensor principal components ( $g_{\text{av}}$ ): ferredoxins with  $g_{\text{av}} \sim 1.96$ , and Rieske clusters with  $g_{\text{av}} \sim 1.91$ .<sup>7</sup> The EPR spectra of clusters reveal a clear rhombic or close to axial symmetry. Variations in  $g$  values observed for the Rieske clusters have been explained on the basis of a ligand-field model of antiferromagnetically coupled iron ions.<sup>8</sup>

Department of Molecular Biophysics, Faculty of Biochemistry, Biophysics and Biotechnology, Jagiellonian University, Kraków, Poland.

E-mail: artur.osyczka@uj.edu.pl; Tel: +48 12 664 63 48

† Electronic supplementary information (ESI) available: Fig. S1: results of equilibrium redox titration of the Fe–S cluster for different forms of cytochrome  $bc_1$ ; Fig. S2: selected results of simulations of X-band CW EPR spectra of the Rieske cluster recorded at 25 K using a single-component model; Fig. S3: temperature dependence of the spin–lattice relaxation rate ( $1/T_1$ ) of the Rieske cluster for the tds-inhibited WT in linearized form for Raman and Orbach processes; Table S1: values of  $g$  and  $g$ -strain components determined from fitting the two-component model to X-band CW EPR spectra (25 K) for different forms of cytochrome  $bc_1$ . See DOI: 10.1039/c5cp02815a



Modifications of  $g$  values are particularly associated with subtle changes in the ligand field around the  $\text{Fe}^{2+}$  ion which is coordinated by histidines. Additionally, the microheterogeneity of the protein environment around the cluster is a source of spread in the ligand field which is manifested as a  $g$ -strain effect in the EPR spectra of the clusters in frozen glassy solutions. A statistical theory for the  $g$ -strain tensor has been developed to describe asymmetry in the line shapes of the iron-sulphur cluster spectra linking the  $g$ -strain with rigidity of the protein core that binds the cluster.<sup>9,10</sup>

The spin-lattice relaxation rate ( $T_1^{-1}$ ) quantitatively describes how fast the energy absorbed by the spin is transferred to the phonons' bath and its value depends on the coupling strength of the relaxing paramagnet to the surrounding environment as well as on the vibrational modes of the lattice. Commonly, the vibrational characteristics of the glassy frozen protein solution, constituting the lattice is described by the Debye model.<sup>11</sup> Temperature dependence of  $T_1^{-1}$  of proteins containing the  $[\text{2Fe-2S}]$  cluster has revealed the existence of direct (one-phonon), second-order Raman and Orbach relaxation processes.<sup>12–14</sup> The second-order Raman process is recognised as a ubiquitous relaxation mechanism for all paramagnetic centres and its efficiency depends on several factors including the extent of spin-orbit coupling and rigidity of the protein that influences the vibrational modes of a paramagnetic centre.<sup>15,16</sup> In general, the larger the spin-orbit coupling (reflected as a deviation of the  $g$ -value from  $g_e$ ) and the less rigid the structure, the higher the efficiency of the Raman process.<sup>17</sup> The Orbach mechanism requires the existence of a low-lying excited state which, in the case of iron-sulphur clusters, originates from antiferromagnetic coupling between high-spin iron ions.<sup>12,18</sup>

The relaxation rates of iron-sulphur clusters have so far mainly been measured for small proteins such as ferredoxins. In these cases, assigning changes in parameters of relaxation to specific structural details of proteins has generally been complicated due to the fact that the comparison involves different proteins coming from different organisms. In this study, we analysed  $T_1^{-1}$  of a reduced Rieske cluster  $[\text{2Fe-2S}]^{2+}$  ( $\text{Fe-S}$ ) of a large membrane protein complex – cytochrome  $bc_1$  (Fig. 1A).<sup>19–21</sup> This protein provides a convenient model to compare  $T_1^{-1}$  of the same metalloprotein exposed to a variety of structural changes associated with modifications of both the local environment of the cluster and the global environment at the level of the whole protein. By the term “local modifications”, here we understand the changes in the structure of hydrogen bonds formed with the cluster or its ligands, while by “global modifications” we understand the changes in the position of the whole iron-sulphur protein head domain (ISP-HD) in relation to other subunits of cytochrome  $bc_1$ .

The  $\text{Fe-S}$  cluster in cytochrome  $bc_1$  is embedded in a water-exposed extrinsic domain (ISP-HD) that naturally undergoes a large-scale movement, inherent in the catalytic cycle of the enzyme. The movement allows the cluster to transfer electrons between the catalytic  $\text{Q}_o$  site in cytochrome  $b$  and heme  $c_1$  on the cytochrome  $c_1$  subunit.<sup>22–26</sup> At one extreme

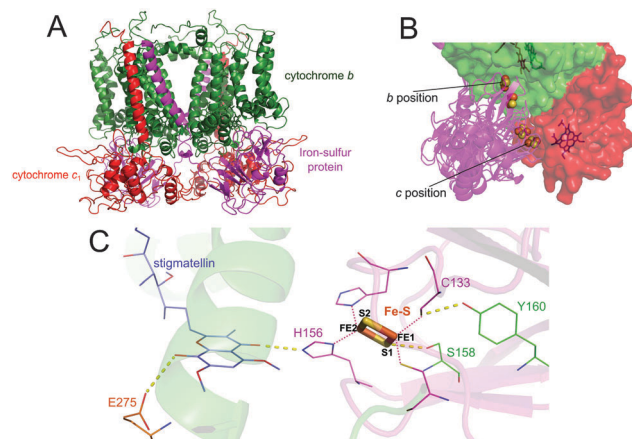


**Fig. 1** Crystal structure of cytochrome  $bc_1$  and structural details of the ISP. (A) A ribbon model of a native cytochrome  $bc_1$  dimer from *Rhodobacter capsulatus* (PDB ID: 1ZRT<sup>20</sup>) containing three catalytic subunits: cytochrome  $b$  – green, cytochrome  $c_1$  – red, and ISP – magenta. (B) A model of one monomer of cytochrome  $bc_1$  with overlaid different positions of the ISP-HD. The  $\text{Fe-S}$  cluster is shown in  $b$ -,  $c$ - and intermediate positions as yellow-red spheres. The sticks represent hemes  $c_1$ ,  $b_L$  and the inhibitor stigmatellin. The positions of the ISP-HD were taken from the structures in the PDB database: 1BCC,<sup>22</sup> 1BE3,<sup>64</sup> 1BGY<sup>64</sup> and 1ZRT.<sup>20</sup> (C) The local environment of the  $\text{Fe-S}$  cluster at the  $b$  position in the presence of stigmatellin that forms the hydrogen bond with cluster-liganding H156. Yellow dashed lines indicate the H bonds and magenta dotted lines represent the bonds between cluster ligands and iron ions of the cluster. Green and magenta ribbons represent cytochrome  $b$  and ISP subunits.

(the so-called “ $b$  position”), the ISP-HD is in close contact with the  $\text{Q}_o$  site and the Rieske cluster interacts with the substrate bound at the site, while at the other extreme (the so-called “ $c$  position”) the ISP-HD is close to heme  $c_1$  (Fig. 1B). It has been shown in previous studies that the redox potential of the cluster varies significantly between these two positions – it is generally more than 100 mV higher at the  $b$  position, compared to the  $c$  position.<sup>25,27</sup>

In isolated non-inhibited wild-type (WT) cytochrome  $bc_1$ , the ISP-HD is distributed between  $b$  and  $c$  position.<sup>26</sup> However, the average position of the ISP-HD can be modified by introducing specific mutations that affect the motion and also by addition of specific inhibitors of cytochrome  $bc_1$ .<sup>26,28,29</sup> Therefore, the properties of the  $\text{Fe-S}$  cluster of cytochrome  $bc_1$  can be studied under a variety of conditions in which the position of the cluster can be controlled.

Here, we performed a detailed analysis of the spin-lattice relaxation rate of the Rieske cluster of cytochrome  $bc_1$  isolated from *Rhodobacter capsulatus* under a variety of conditions to determine the basic parameters of the mechanisms that govern the relaxation between 5 K and 120 K particularly, the Orbach energy and Debye temperature. We compared the effect of point mutations S158A and Y160W that remove the specific H bonds in the proximity of the cluster. We also investigated the effect on the efficiency of the Raman process of changes in the global distribution of positions of the ISP-HD modified by using specific inhibitors and mutations.



## Materials and methods

### Bacterial strains, plasmids, and general molecular genetic techniques

*Rb. capsulatus* strains and *E. coli* (HB101) were grown in MPYE (mineral–peptone–yeast extract) and LB media, respectively, supplemented with appropriate antibiotics as needed.<sup>30</sup> Photosynthetic growth of *Rb. capsulatus* strains was tested on MPYE plates using anaerobic jars (GasPak System, BD) at 30 °C under continuous light. *Rb. capsulatus* strains with mutated cytochrome *bc*<sub>1</sub> were generated as described previously,<sup>31</sup> using the genetic system developed by Dr F. Daldal (University of Pennsylvania, Philadelphia, USA). The templates containing the desired mutations were obtained using the QuikChange<sup>®</sup> protocol (Stratagene). Changes in the *petA* gene (coding for the ISP subunit) resulting in the mutations S158A or Y160W were introduced by PCR using DNA as a template: pPET1 (for construction of single mutants S158A or Y160W), pPET1 containing mutations for +1Ala or +2Ala insertions<sup>23</sup> (for construction of double mutants S158A +1Ala or S158A +2Ala, respectively). The 1 kb *Bst*XI/*Xma*I fragments containing the desired mutations (and no other mutations, as confirmed by DNA sequence analysis) were exchanged with their wild-type counterparts in pMTS1 to construct mutated variants of pMTS1. These were used as expression vectors in *Rb. capsulatus* cells. They were introduced into the MT-RBC1 strain (*petABC*-operon deletion background) *via* triparental crosses as described in ref. 31. In each case, the presence of engineered mutations was confirmed by sequencing the plasmid DNA isolated from the mutated *Rb. capsulatus* strains.

### Biochemical procedures

The cytochrome *bc*<sub>1</sub> complex was isolated from purple bacteria *Rb. capsulatus* grown under semiaerobic conditions, according to the procedure described previously in ref. 32. The concentration of the isolated protein (per cytochrome *c*<sub>1</sub> content) was determined spectrophotometrically using ascorbate-reduced minus ferricyanide-oxidised differential spectra and an extinction coefficient  $\epsilon_{552-542\text{nm}} = 20 \text{ mM}^{-1}$ . All forms of cytochrome *bc*<sub>1</sub> were dialysed against buffer containing 50 mM bicine pH 8, 100 mM KCl, 1 mM EDTA, 20% (v/v) glycerol and 0.01% dodecyl maltoside. Inhibitors tridecyl stigmatellin (tds), myxothiazol (myx), famoxadone (fam), atovaquone (ato) and antimycin (ant) were added from DMSO stock solution to obtain a molar excess over the protein. The inhibitors were purchased from Sigma-Aldrich, except for tds, which was a generous gift from Dr N. Fisher. All forms of cytochrome *bc*<sub>1</sub> bind inhibitors with similar affinities as inferred from enzymatic turnover assays and light-induced electron transfer measurements (data not shown).

The measurements of the enzymatic activity of the different forms of cytochrome *bc*<sub>1</sub> were performed as described in ref. 33 using 20  $\mu\text{M}$  horse cytochrome *c*, 20  $\mu\text{M}$  decylubihydroquinone and 10–100 nM of the enzyme.

Equilibrium redox titrations of the Fe–S cluster were performed on the isolated protein at pH 8. To minimise the pH shift upon freezing the bicine buffer was used.<sup>34</sup> The following redox mediators were applied: tetrachlorohydroquinone, diaminodulol, 1,2-napthoquinone-4-sulfonate, phenazine methosulphate, phenazine

ethosulphate, 1,2-napthoquinone. Ambient redox potential was adjusted by addition of small aliquots of potassium ferricyanide or sodium dithionite solutions. For each point of ambient potential a small portion of the sample was anaerobically transferred to an EPR tube and frozen in liquid nitrogen. Spectra of the titrated protein were subsequently measured by CW EPR at 20 K and the redox potential was determined by fitting the Nernst equation to the data points (Fig. S1, ESI†).

Prior to EPR measurements, all samples of cytochrome *bc*<sub>1</sub>, except for those prepared for redox titration, were reduced with sodium dithionite to keep all the protein cofactors in reduced state. After reduction, samples were frozen and stored in liquid nitrogen until used.

### EPR measurements

EPR spectroscopy was performed on a Bruker Elexsys E580 spectrometer operating at X- and Q-bands using similar equipment and settings as described previously in ref. 26 and 35. CW spectra were recorded at the X-band over the temperature range 20–120 K using a non-saturating microwave power.

### Inversion recovery measurements at 5–25 K

Pulse EPR experiments were carried out in a Bruker Q-band resonator ER5107D2. Inversion recovery (IR) measurements were performed at 5–25 K using a pulse sequence:  $\pi-t_d-\pi/2-t-\pi$  with a constant  $t = 160 \text{ ns}$ . The initial  $t_d = 160 \text{ ns}$  was incremented to cover the whole recovery curve after the inverting  $\pi$  pulse. Such a sequence of pulses yields an overall dead time of IR measurement of  $\sim 500 \text{ ns}$ . Within the considered temperature range the relationship:  $T_1 \gg T_2$  is valid, therefore transverse relaxation does not affect the measured IR curves.<sup>26</sup> The lengths of microwave pulses  $\pi/2$  and  $\pi$  were set to 20 and 40 ns, respectively and the microwave pulse power was adjusted to obtain the maximum amplitude of the spin echo. Above 25 K the relaxation becomes very fast and most of the recovery takes place within the experimental dead time, therefore only residual slow-relaxing components of the recovery can be detected. Above 30 K the spin-echo signal becomes virtually undetectable.

The measured IR curves were non-exponential, indicating the distribution of relaxation rates or spectral diffusion. To evaluate the possible effect of spectral diffusion on the recorded IR trace we performed measurements in which the first inverting  $\pi$  pulse was replaced with a saturating picket-fence of microwave pulses, or with a single saturating long-pulse. However, in all cases the shape of recovery curves remained unchanged. The experimental IR curves were mathematically modelled using a stretched exponent function:

$$Y(t) = a \cdot \exp \left[ - \left( \frac{t}{\tau} \right)^\beta \right] + y_0$$

where  $\tau$  and  $\beta$  represent the time constant of the process and the stretching parameter, respectively.

The average spin–lattice relaxation rate was then calculated using the equation:

$$\frac{1}{T_1} = \left[ \Gamma(\beta^{-1}) \frac{\tau}{\beta} \right]^{-1}$$

where  $\Gamma$  is the gamma function.<sup>36</sup>



For tds-treated WT, S158A and Y160W and non-inhibited S158A, WT, Y160W, and +2Ala, S158A +1Ala IR curves were measured at  $g_z$ ,  $g_y$  and  $g_x$  transitions. In all cases the obtained  $T_1$  values depended on their position in the Fe-S spectrum, proving the anisotropic character of the relaxation. In the presence of tds, the spin-lattice relaxation rate increased in the order:  $(1/T_1)_{g_x} < (1/T_1)_{g_y} < (1/T_1)_{g_z}$ , while for non-inhibited enzymes a different relationship occurred:  $(1/T_1)_{g_y} < (1/T_1)_{g_x} < (1/T_1)_{g_z}$ . The origin of these changes in the relaxation anisotropy upon addition of tds is not known but probably it could be associated with the formation of the hydrogen bond between the inhibitor and the cluster liganding histidine 156. In further analyses only  $T_1$  determined at  $g_y$  transition was considered.

### Analysis of CW EPR spectra and determination of $T_1$ for temperatures above 80 K

At temperatures higher than 40 K,  $T_1$  shortens and drives transverse relaxation ( $T_2 = T_1$ ). As temperature increases, the homogeneous broadening of the individual resonance lines increases with  $T_1^{-1}$ , affecting the CW EPR powder spectrum. Estimation of  $g$  and  $g$ -strain tensors, as well as the temperature-dependent Lorentzian broadening for a particular variant of cytochrome  $bc_1$  results from the fitting of the simulated EPR spectrum to experimentally measured traces.

A model of “powder” EPR spectrum simulation, adequate for frozen solutions of metalloproteins (with  $S = 1/2$ ) was developed by Hagen.<sup>37</sup> In our simulations we implemented the basic foundations of Hagen’s algorithm: the  $g$ -strain tensor was defined in the  $g$ -values space, and its components (up to six) determined an orientation-dependent Gaussian linewidth  $\gamma_G(\theta, \varphi)$  of the resonance transition at  $g_{\text{eff}} = g(\theta, \varphi)$ . In addition, the tensor  $L$  (expressed in terms of  $g$ -values space) was incorporated into the model to account for the presence of anisotropic homogeneous broadening. The principal values of the  $L$  tensor were used to calculate the effective value of the Lorentzian linewidth  $\gamma_L(\theta, \varphi)$  using an expression analogical to that used for the Gaussian linewidth  $\gamma_G(\theta, \varphi)$ . The subsequent lineshape for a given resonance line resulted from convolution of the Gaussian and Lorentzian broadening mechanisms which for practical reasons was approximated by the pseudo-Voigt profile.<sup>38,39</sup> The simulated EPR spectrum was created as a superposition of all the calculated signals originating from particular centres that were randomly oriented with respect to the applied magnetic field. This was performed as an orientation-weighted sum over a sphere represented by a SOPHE grid,<sup>40,41</sup> which typically consisted of 1000 orientations. Each spectrum was transformed from the  $g$ -value domain to the magnetic field domain using proper renormalization formulas. All numerical simulations of the EPR spectra were implemented in a Matlab environment, using the original procedures (available upon request). The values of  $g$ ,  $g$ -strain and  $L$  were determined for all examined cytochrome  $bc_1$  samples as the “best fit” parameters. Initially, the simulated spectra were fitted using the Simplex method and then further optimised using the Levenberg–Marquardt algorithm (LMA). For temperatures where  $T_2 = T_1$ , based on the fitted values of the  $L$  tensor, the spin-lattice

relaxation rates for each line  $i = x, y, z$  were calculated using the formula:

$$\frac{1}{T_{1i}} = 2\pi\nu \frac{L_i}{g_i}$$

where  $\nu$  is the microwave frequency,  $L_i$  denotes the principal value of the  $L$  tensor (full width at half maximum (FWHM) of the Lorentzian line in the  $g$ -value domain) and  $g_i$  is the principal value of the  $g$ -tensor.

In the case of multicomponent spectra the average relaxation rate was calculated as the weighted mean value of relaxation rates obtained from the  $L$  tensor for each spectral component.

### Analysis of temperature dependence of the relaxation rate of the Rieske cluster

Spin-lattice relaxation rates of different forms of cytochrome  $bc_1$ , determined for the whole temperature range 5–120 K, were fitted using LMA as the sum of three mechanisms: direct, Raman and Orbach:

$$\frac{1}{T_1} = C_{\text{dir}}T + C_{\text{Ram}}\left(\frac{T}{\theta_D}\right)^9 J_8\left(\frac{\theta_D}{T}\right) + C_{\text{Orb}} \cdot E_{\text{Orb}}^3 [\exp(E_{\text{Orb}}T^{-1}) - 1]^{-1}$$

In this equation,  $C_{\text{dir}}$ ,  $C_{\text{Ram}}$  and  $C_{\text{Orb}}$  are the efficiencies of direct, Raman and Orbach processes, respectively.  $\theta_D$  and  $E_{\text{Orb}}$  denote the Debye temperature and Orbach energy, respectively. The transport integral  $J_8$  was substituted with an analytical approximation, as described in ref. 42 which allowed us to fit  $\theta_D$  as an independent parameter. The uncertainty levels of the determined “best-fit” parameters were obtained from square roots of diagonal elements of the covariance matrix, calculated by LMA. To compare  $C_{\text{Ram}}$  for different samples we performed additional fitting of the data obtained in the temperature range 10–25 K with the  $\theta_D$  value fixed at 107 K, which is the average Debye temperature determined for all samples.

To compare spectral anisotropy between different samples we introduced a phenomenological parameter  $A$ , that provides the average (over the whole EPR spectrum) measure of spin-orbit coupling.  $A$  is defined as:

$$A = \sqrt{\sum_i^n [(g_e - g_i)^2 \cdot f(g_i) \cdot \Delta g]}$$

where  $i$  is a consecutive point of a simulated spectrum in the  $g$ -value domain,  $n$  is the total number of points of the digitised spectrum,  $f(g_i)$  is the amplitude of the absorption spectrum at  $g_i$  position,  $g_e$  is the  $g$ -value of the free electron,  $g_i$  is the consecutive  $g$ -value and  $\Delta g$  is the resolution. The value of “ $A$ ”, calculated on the basis of the EPR spectrum for a disordered sample, is sensitive not only to the deviation of the adequate  $g$ -tensor from  $g_e$ , but also to the sample-specific distribution  $f(g_i)$ . Thus, the proposed formula more reliably reflects the effective strength of spin-orbit coupling and can differentiate the samples with similar  $g$ -tensors but different EPR spectrum shapes.





**Table 1** Relative equilibrium redox midpoint potentials of the Fe–S cluster in the WT and mutants of cytochrome *bc*<sub>1</sub>, the ability of the enzyme to support photosynthetic growth of *Rhodobacter capsulatus* cells and enzymatic activity of the enzyme

Form	$\Delta E_{m,pH8}$ [mV]	Photosynthetic growth	Turnover rate of cytochrome <i>c</i> reduction [ $s^{-1}$ ] $\pm$ st. error
WT	0	+++	140 $\pm$ 5
+1Ala	+13	+++	144 $\pm$ 7
+2Ala	+89	–	4.2 $\pm$ 0.2
S158A	–133	+	18.1 $\pm$ 0.6
Y160W	–103	++	11.9 $\pm$ 0.2

## Results and discussion

### Effect of mutations and inhibitors on the position of the ISP-HD and redox properties of the Fe–S cluster

We analysed the properties of the ISP in the presence of various mutations and/or inhibitors of quinone catalytic sites. All these factors introduced structural changes in the local environment of the Fe–S cluster and some of them also influenced the average distribution of ISP-HD positions. The mutations affecting the motion included insertions of one or two Ala residues in position 46<sup>23,24</sup> (+1Ala or +2Ala) leading to a shift of various degrees of the population of the ISP-HD towards the cytochrome *b* subunit (to the *b* position) (Fig. 1B). In +1Ala, the ISP-HD is arrested at the *b* position for at least several milliseconds which leads to only a slight decrease in the enzymatic activity of cytochrome *bc*<sub>1</sub>.<sup>27,29,43,44</sup> In +2Ala the ISP-HD is arrested at this position for hundreds of milliseconds, which relegates the electron transfer between *Q*<sub>o</sub> and heme *c*<sub>1</sub> at the time scale of seconds severely inhibiting the enzymatic activity. The mutations in the local environment of the Fe–S cluster included replacement of either S158 to Ala or Y160 to Trp (Fig. 1C). S158A removes the hydrogen bond between the –OH group of serine and the S1 sulphur of the cluster, whereas changing Y160 to Trp not only removes the hydrogen bond between the –OH group of tyrosine and the sulphur atom of the cluster liganding C133, but also slightly shifts the positions of amino acid side chains around the cluster shell to accommodate a relatively large tryptophane residue.<sup>45–48</sup> S158A was tested alone (single mutant S158A) or in combination with +1Ala and +2Ala (double mutants S158A +1Ala and S158A +2Ala, respectively).

As shown in Table 1, S158A and Y160W decreased  $E_m$  by  $\sim 133$  and  $\sim 100$  mV, respectively. This is reflected in the lower enzymatic activity and the slower growth rate of bacterial cells under photosynthetic conditions.† The changes in the  $E_m$  of S158A and Y160W are associated with the removal of hydrogen bonds in the vicinity of the cluster as anticipated from inspection of the crystal structure of analogous mutants in *Rhodobacter sphaeroides* and biochemical studies of the mutated ISP from other organisms.<sup>46–49</sup>

Table 1 shows that +1Ala and +2Ala also influence the  $E_m$ , as reported earlier.<sup>27</sup> When the ISP-HD is in the *b* position, the redox potential of Fe–S is higher compared to the potential of

Fe–S in other positions:<sup>27</sup> thus, in +2Ala, in which almost the entire population is in the *b* position, the redox potential is elevated by  $\sim 90$  mV, while in +1Ala, in which the population at the *b* position is larger than in the WT but less than is the case for +2Ala, the potential is elevated by  $\sim 20$  mV. The increase in the redox potential upon shifting the ISP-HD to the *b* position (+1Ala or +2Ala) appears to be independent from the effect of hydrogen bonding as it is also observed for mutants with the shifted ISP-HD and lacking specific H bonds (see example S158A vs. S158A +1Ala in Fig. S1, ESI†). The origin of the change in redox potential of Fe–S related to the change in position of the ISP-HD is still not clear,<sup>25,50</sup> but it is likely related to distortions of the active site upon binding the ISP-HD to the *Q*<sub>o</sub> site that modifies the ionisation potential of the cluster.<sup>4,51</sup>

Inhibitors of the *Q*<sub>o</sub> catalytic site included tds, ato, fam and myx.<sup>52,53</sup> The first three inhibitors (tds, ato, and fam) fix the ISP-HD at the *b* position, which can occur with (tds and ato) or without (fam) formation of a hydrogen bond between the inhibitor and cluster-liganding H156 residue. Myxothiazol has the opposite effect; it shifts the domains out of the *b* position.<sup>54</sup>

### Inversion recovery rates of the Rieske cluster at 12 K

Fig. 2A shows inversion recovery curves measured at 12 K at the *g*<sub>y</sub> transition of the Fe–S cluster for samples in which the distribution of positions of the ISP-HD was modified by +1Ala mutation or by using inhibitors tds or myx. The recovery rate increases in the order WT + tds < +1Ala < WT < WT + myx ( $11.3 \times 10^3$ ,  $12.1 \times 10^3$ ,  $15.2 \times 10^3$ , and  $18.3 \times 10^3$  s<sup>–1</sup>, respectively, at 12 K) and appears to correlate with the shift of the ISP-HD out of the *b* position: the domains that are closer to the *b* position exhibit slower recovery rates.

The effect of point mutations S158A and Y160W on *T*<sub>1</sub> was initially tested in the presence of tds to eliminate the possible influence from changes in the distribution of ISP-HD positions on *T*<sub>1</sub>. The relaxation rate for these samples increased in the order of S158A + tds < Y160W + tds < WT + tds ( $4.5 \times 10^3$ ,  $6.1 \times 10^3$  and  $11.3 \times 10^3$  s<sup>–1</sup>, at 12 K respectively) (Fig. 2B). This effect must result from modifications in the local protein structure near the Fe–S cluster binding site, in particular the lack of specific hydrogen bonds in the mutants.

### Analysis of CW EPR spectra of the Fe–S cluster at low temperature

The modification of the cytochrome *bc*<sub>1</sub> structure caused by mutations and/or inhibitors affected the features of CW EPR spectra of the Rieske cluster in particular samples; however, the general rhombic shape was preserved in all cases (see examples in Fig. 3).

Simulation of CW EPR spectra at 25 K allowed us to estimate the principal *g* tensor and *g*-strain values that define the inhomogeneous line broadening and the number of components in the particular CW spectrum (see Table S1 in the ESI†). Introducing off-diagonal elements of the *g*-strain tensors did not improve the fits thus in all cases only principal *g*-strain values were considered.

† *Rb. capsulatus* obligatorily requires functional cytochrome *bc*<sub>1</sub> to support photosynthetic growth of the bacteria in the absence of oxygen; therefore growth under these conditions reflects the general activity of the enzyme.



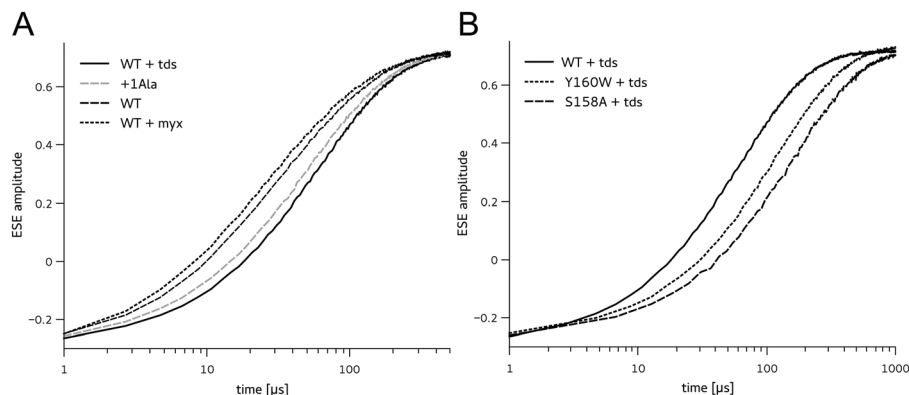


Fig. 2 Semi-log plot of inversion recovery curves measured at the  $g_y$  transition of the Fe–S cluster at 12 K. Comparison of recovery curves for cytochrome  $bc_1$  with different average positions of the ISP-HD in the absence of point mutations (A) and for S158A or Y160W mutants with the ISP-HD arrested at the  $b$  position by treatment with tds (B).

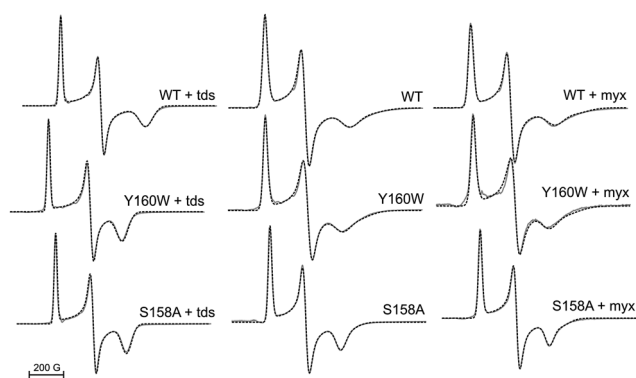


Fig. 3 Simulation of X-band CW EPR spectra measured at 25 K of the Fe–S cluster for WT, S158A and Y160W mutants. Spectra from left to right correspond to the forms in which the average distance of the Fe–S cluster from the  $b$  position increases. Solid grey and dashed black lines show experimental and simulated spectra, respectively.

The use of one spectral component was sufficient to simulate spectra only for samples in which the ISP-HD was fixed at the  $b$  position due to the presence of mutation (+2Ala, S158A +2Ala) or inhibitor tds (WT + tds, S158A + tds, Y160W + tds). This observation suggests that tds and +2Ala mutants arrest the ISP-HD at the  $b$  position in such a way that the population of the Fe–S clusters is uniform and single-component. Other inhibitors that also restrict the motion of the ISP-HD (ato, fam) required the introduction of two components, with clearly different  $g$ -tensors, to reproduce the experimental spectra. In the presence of ato, addition of  $\sim 18\%$  of the second component was needed, while in the presence of fam, the two components contributed almost equally. The difference in the number of components between tds and ato or fam can be explained by the fact that ato and fam are not as strong inhibitors as stigmatellin and that the hydrogen bond between the inhibitor and ISP-HD is weaker (ato)<sup>55–57</sup> or not formed at all (fam).<sup>52,58,59</sup> The remaining spectra also required more than one component to obtain good fits but generally two components were sufficient to reproduce all experimental spectra. Fig. S2 (ESI†) shows the inadequacy of selected single-component fits.

Point mutations S158A and Y160W led to an increase in  $g$  values and a decrease in both average spectral anisotropy and  $g$ -strain values of the Fe–S cluster, when compared to WT. This effect is associated with the changes in the electronic configuration due to modifications of hydrogen bonds around the Fe–S cluster. The addition of myx to the samples led to only small changes in  $g$  values and  $g$  strain. The representative results of spectral simulations for the WT, S158A and Y160W, in combination with tds and myx are shown in Fig. 3.

#### Spin-lattice relaxation rate obtained from simulation of CW spectra at higher temperature

For simulations of spectra registered in the temperature range 80–120 K only homogeneous broadening was considered to change upon increase in the temperature. The other parameters (*e.g.*  $g$  values,  $g$  strain, number of components, *etc.*) were fixed at values established from simulations of the respective spectra at 25 K. This assumption was justified by the fact that temperatures below 120 K are still low enough to keep the protein structure unchanged in comparison to the structures at 25 K.

In several cases, the fitting of the CW spectra using a model with isotropic Lorentzian broadening led to unacceptably poor fits (see examples for WT and WT + myx shown in Fig. 4). Given that, and also taking into account the anisotropy of IR rates, we concluded that the broadening of the lines must be described by the anisotropic Lorentzian linewidth. Indeed, the anisotropic model of Lorentzian broadening significantly improved the fits (Fig. 4). Clearly, at higher temperatures the relaxation follows the anisotropic trend observed at low temperatures and this anisotropy is even more pronounced.

#### Mechanisms of spin-lattice relaxation of the Fe–S cluster

A physical explanation of the spin-lattice relaxation process must refer to the electronic states of the exchange-coupled diiron cluster and the vibrational properties of the lattice. When modifications of the structure surrounding the paramagnetic centre affect the protein vibrational modes, the measured  $T_1$  values differ between variants of cytochrome  $bc_1$ . Within the investigated temperature range (5–120 K) we consider the



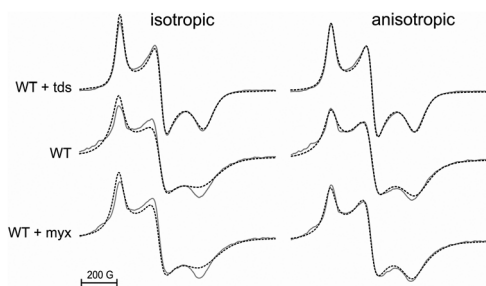


Fig. 4 CW EPR spectra of the Fe–S cluster measured at 100 K for non-inhibited WT cytochrome *bc*<sub>1</sub>, treated with tridecyl-stigmatellin (tds) and myxothiazol (myx). Solid grey and dashed black lines show experimental and simulated spectra, respectively. Left and right columns show the results of fitting the same experimental data with a model assuming isotropic and anisotropic Lorentzian broadening of the lines, respectively.

existence of three relaxation mechanisms: direct, Orbach, and second-order Raman processes, as inferred from the characteristic temperature dependence of  $1/T_1$  (see Fig. S3 (ESI<sup>†</sup>) for a

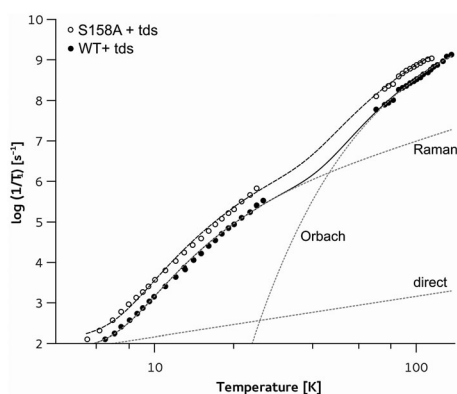


Fig. 5 Log-log plot of temperature dependence of the spin–lattice relaxation rate of the Fe–S cluster obtained for tds-treated WT and S158A (open and closed symbols, respectively). The solid line shows the fit of direct, Raman and Orbach processes to experimental data. Dashed lines show the contribution from these three processes to the relaxation of Fe–S in the mutant S158A in the presence of tds.

linear representation of the relaxation rate typical for Raman or Orbach processes).

In Fig. 5, two representative curves of the relaxation rate as a function of temperature 5–120 K are shown. In the range 10–25 K,  $1/T_1$  increases with approximately a sixth power of temperature, indicating domination of the second-order Raman process. Above 80 K this dependence is exponential, suggesting the contribution from the Orbach process, which starts to dominate upon an increase in temperature. At the lowest temperatures (below 10 K), a contribution from the direct process can be recognised from the observation that IR curves are frequency-dependent (the relaxation rates measured at the Q band are higher than those measured at the X band). This frequency-dependence becomes undetectable upon an increase in the temperature as other mechanisms prevail (data not shown). Fig. 5 also shows representative fits of the sum of these three mechanisms to the experimental data points yielding parameters shown in Table 2. For all forms of cytochrome *bc*<sub>1</sub> investigated here, the Debye temperature falls within the range 100–120 K (with an average value of 107 K), which is in agreement with values reported for frozen glassy solutions of proteins.<sup>15</sup> The Orbach energy falls within the range  $\sim 350$ – $550$  K with an average value of  $\sim 450$  K ( $\sim 300$  cm<sup>−1</sup>), which also is in the same order as previously reported values for ferredoxins.<sup>14,60</sup>

Comparison of the WT with S158A and Y160W indicates that the Orbach energy increases in these mutants (353 K for WT vs. 447 and 554 K in S158A and Y160W, respectively), suggesting an increased antiferromagnetic coupling between Fe ions in the cluster. This effect is likely to be related to subtle changes in the geometry of the Fe–S cluster particularly in terms of the Fe–S distance and/or Fe–S–Fe angle.<sup>61</sup> Inhibitors and mutations affecting the motion of the ISP-HD also influence the Orbach energy, but at this point it is difficult to find a clear tendency for these changes (Table 2).

### Efficiency of Raman relaxation in different forms of cytochrome *bc*<sub>1</sub>

Parameters describing the efficiency of Raman relaxation and Debye temperature are correlated.<sup>62</sup> This means that changes

Table 2 Parameters of spin–lattice relaxation for different forms of the Rieske cluster

Group	Sample	$C_{\text{Dir}} [\text{s}^{-1} \text{K}^{-1}]$	$C_{\text{Ram}} [\text{s}^{-1} \text{K}^{-9}] \times 10^{-10}$	$\theta_{\text{D}} [\text{K}]$	$C_{\text{orb}} [\text{s}^{-1} \text{K}^{-3}]$	$\Delta_{\text{orb}} [\text{K}]$
A	WT	$24.0 \pm 3.2$	$1.59 \pm 0.16$	$108 \pm 4$	$966 \pm 130$	$353 \pm 29$
	WT + tds	$24.8 \pm 2.9$	$1.24 \pm 0.11$	$103 \pm 3$	$612 \pm 59$	$398 \pm 25$
	WT + myx	$33.9 \pm 5.7$	$1.86 \pm 0.22$	$109 \pm 5$	$1052 \pm 225$	$406 \pm 46$
	WT + ato	$40.3 \pm 9.4$	$0.91 \pm 0.17$	$111 \pm 6$	nd	nd
	WT + fam	$23.0 \pm 2.3$	$0.98 \pm 0.07$	$104 \pm 3$	nd	nd
	WT + ant + myx	$22.7 \pm 6.8$	$1.96 \pm 0.24$	$110 \pm 5$	nd	nd
	+1Ala	$27.1 \pm 2.9$	$1.39 \pm 0.12$	$102 \pm 3$	$907 \pm 144$	$505 \pm 28$
	+2Ala	$31.8 \pm 4.0$	$0.913 \pm 0.090$	$108 \pm 3$	$444 \pm 43$	$410 \pm 25$
B	S158A	$14.3 \pm 2.4$	$0.441 \pm 0.066$	$118 \pm 5$	$234 \pm 49$	$447 \pm 48$
	S158A + tds	$14.8 \pm 1.2$	$0.411 \pm 0.031$	$109 \pm 3$	$364 \pm 24$	$465 \pm 16$
	S158A + myx	$16.0 \pm 1.8$	$0.77 \pm 0.08$	$101 \pm 3$	nd	nd
	S158A +1Ala	$17.1 \pm 2.0$	$0.71 \pm 0.06$	$99 \pm 3$	$345 \pm 26$	$523 \pm 16$
	S158A +2Ala	$21.5 \pm 2.3$	$0.455 \pm 0.046$	$108 \pm 3$	$222 \pm 22$	$470 \pm 30$
C	Y160W	$20.6 \pm 3.3$	$1.09 \pm 0.13$	$108 \pm 4$	$4290 \pm 1077$	$554 \pm 64$
	Y160W + tds	$14.4 \pm 1.2$	$0.599 \pm 0.041$	$107 \pm 3$	$469 \pm 34$	$425 \pm 18$
	Y160W + myx	$23.1 \pm 4.0$	$1.15 \pm 0.13$	$104 \pm 4$	nd	nd



in  $C_{\text{Ram}}$  can be compensated by changes in  $\theta_D$ . Therefore, to compare  $C_{\text{Ram}}$  for different samples,  $\theta_D$  was kept constant at 107 K and only Raman efficiency was fitted yielding  $C_{\text{Ram}}'$  values.

The point mutation around the Fe-S cluster (S158A or Y160W) has a dominant effect on the relaxation rates thus, the influence of other factors differentiating the samples was further examined within 3 groups: A – encompassing WT variants with the presence or absence of different inhibitors and +1Ala, +2Ala insertions; B – S158A variants with or without inhibitors or +1Ala, +2Ala insertions; and C – Y160W variants with or without inhibitors. The values of  $C_{\text{Ram}}'$  were compared within each of these groups.

Such analysis revealed the following regularities. When the ISP-HD is fixed at the *b* position due to the presence of tds, ato, fam or mutation +2Ala, the efficiency of the Raman process decreases. On the other hand, the inhibitors that shift the ISP-HD distribution out of the *b* position (myx, and myx + ant) cause the  $C_{\text{Ram}}'$  to increase in comparison to non-inhibited enzymes. These results suggest that the relaxation efficiency of the Raman process for the Fe-S cluster in cytochrome *bc*<sub>1</sub> generally correlates with an increase in the average distance of the ISP-HD from the *b* position.

The efficiency of Raman relaxation generally increases with an increase in spin-orbit coupling, which is proportional to the difference between *g*-values and  $g_e = 2.0023$ . It is also known that for paramagnetic centres with comparable spin-orbit coupling the efficiency is smaller for structures that are more rigid. Therefore, to estimate possible contributions from spin-orbit coupling and protein rigidity, we analysed the dependence of  $C_{\text{Ram}}'$  on the average spectral anisotropy *A* (Fig. 6).

The experimental data, depicted in Fig. 6, confirmed the expected general tendency for an increase in  $C_{\text{Ram}}'$  with growing spin-orbit coupling. However, close inspection of the data in Fig. 6 reveals several cases for which an increase in spectral anisotropy does not lead to an increase in  $C_{\text{Ram}}'$  (for example  $C_{\text{Ram}}'$  in S158A +1Ala = S158A = Y160W + tds, S158A +2Ala = S158A + tds or +2Ala = WT + fam = WT + ato) or an increase in

$C_{\text{Ram}}'$  is not associated only with a change in spectral anisotropy (for example,  $C_{\text{Ram}}'$  in S158A + tds < S158A < S158A + myx, WT < WT + myx < WT + ant + myx). There is even a case for which  $C_{\text{Ram}}'$  decreases while spectral anisotropy increases (compare  $C_{\text{Ram}}'$  in a series +1Ala > Y160W + myx > WT + tds > Y160W > WT + ato).

Considering the black points in Fig. 6 (all describing different forms of S158A), one can predict that of the two forms of the Fe-S cluster with the ISP-HD arrested at the *b* position (S158A +2Ala and S158A + tds) the one, with the inhibitor tds, is probably more rigid. On the other hand, the Fe-S core becomes less rigid as the population of the cluster is shifted out of the *b* position ( $C_{\text{Ram}}'$  in S158A + tds < S158A < S158A + myx). A similar trend can be observed when the ISP-HD in the WT is shifted out of the *b* position (compare  $C_{\text{Ram}}'$  for WT < WT + myx < WT + ant + myx – blue points in Fig. 6). This suggests that the rigidity of the Fe-S cluster changes depending on its position, and it is generally larger when Fe-S is in contact with the catalytic Q<sub>o</sub> site (*b* position). In addition, in the *b* position the rigidity appears to be modified by the presence and the type of inhibitor that occupies the site (compare for example: +2Ala, WT + fam and WT + ato). This is probably related to the capability of an inhibitor to create a hydrogen bond with cluster-liganding H156.

Interestingly, Fig. 6 shows examples of  $C_{\text{Ram}}'$  values that are negatively correlated with spectral anisotropy. This is best seen for the series +1Ala, Y160W + myx, WT + tds, Y160W and WT + ato. To explain this result, we propose that the effect of an increase in spin-orbit coupling is compensated or even dominated by the progressive increase in the rigidity of the protein.

### Effect of changes in hydrogen bonding on the Raman relaxation of the Fe-S cluster

The series of samples studied here allowed us to evaluate the effect of two types of hydrogen bonds on the efficiency of Raman relaxation. The first type involved intramolecular H bond located within the core of the Fe-S cluster (between the OH group of S158 and S1 of the cluster or the OH group of Y160 with the S atom of cluster-liganding C133), while the second type involved the intermolecular bond between the inhibitor occupying the catalytic Q<sub>o</sub> site within the cytochrome *b* subunit and cluster-liganding H156 on the ISP-HD.

Removing the intramolecular H bond in S158A or Y160W leads to a decrease in  $C_{\text{Ram}}'$  which may result from changes in vibrational modes and/or spin-orbit coupling. While at this stage separating contributions from these two factors is difficult, one can expect that, if the effect of changes in vibrational modes is significant, then the intramolecular H bond provides an additional channel to transfer vibrations from the surroundings to the paramagnetic centre (Fe-S). On the other hand, an addition of the intermolecular H bond in the presence of the inhibitor may lead to an increase in the rigidity of the Fe-S binding core, probably due to the introduction of an additional constraint to the motion when two subunits of cytochrome *bc*<sub>1</sub> (cytochrome *b* and ISP) are in close contact and are additionally stabilised by interactions with the bound inhibitor. However this

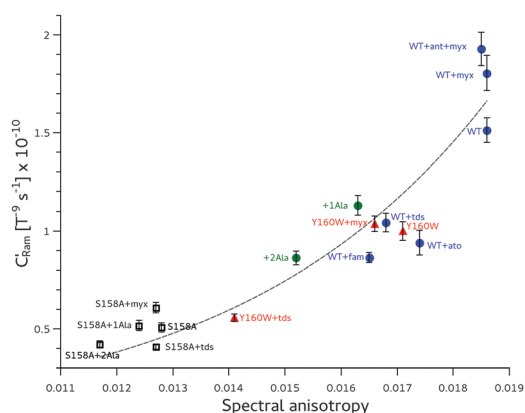


Fig. 6 Efficiency of the Raman process ( $C_{\text{Ram}}'$ ) plotted as a function of spectral anisotropy determined for the WT (blue) and mutants +1Ala and +2Ala (green), Y160W (red) and S158A (black) in combination with different inhibitors that influence the average position of the ISP-HD. The black dotted line represents the exponential growth fit to guide eye.





interpretation should be treated with caution, as at this level we have no data on the vibrational modes of the lattice for the different variants of the cytochrome  $bc_1$ .

## Concluding remarks

In this study, we examined changes in  $T_1$  of the Rieske cluster in cytochrome  $bc_1$  induced by several structural factors. Removal of H bonds in S158A or Y160W significantly increases  $T_1$  of the Fe–S cluster. A somewhat weaker but similar effect was observed when the distribution of the positions of the ISP-HD (induced by mutations +1Ala, +2Ala or inhibitors) was shifted to the  $b$  position (to catalytic  $Q_o$  site) and this effect was independent of changes in H bonding. Therefore, the measurement of  $T_1$  offers a way to monitor the general position of the ISP-HD with a reduced Fe–S cluster, irrespective of the redox state of the remaining cofactors of cytochrome  $bc_1$ . This is provided that mutants with the same intramolecular H bonding pattern are compared. This means that this is complementary to the previously described method of monitoring the ISP-HD distribution that was based on the measurement of the phase-relaxation-enhancement of the Fe–S cluster induced by the relaxation of heme  $b_L$ . The latter method obligatorily required the presence of oxidised heme  $b_L$  that can interact with the Rieske cluster *via* dipolar interaction.<sup>26</sup>

The spin–lattice relaxation rate of the Fe–S cluster revealed the existence of significant anisotropy, which becomes more pronounced as temperature increases. Above 80 K, it is so large that simulation of the CW EPR spectra of the cluster must include the anisotropic  $L$  tensor which defines different magnitude of Lorentzian broadening for the  $g_z$ ,  $g_y$ , and  $g_x$  transitions.

The temperature dependence of the relaxation rates can be explained by assuming the presence of direct (below 5 K), Raman (dominating between  $\sim 10$ –25 K) and Orbach (dominating above  $\sim 80$  K) processes. The presence of these mechanisms in the Rieske cluster of cytochrome  $bc_1$  is in agreement with mechanisms described for spin–lattice relaxation of other iron–sulphur clusters in small proteins such as ferredoxins.<sup>18,63</sup>

The average Orbach energy reflecting antiferromagnetic coupling of the Rieske cluster in cytochrome  $bc_1$  was approximately 450 K ( $\sim 300\text{ cm}^{-1}$ ) which is similar to other iron–sulphur proteins. We found that eliminating specific H bonds between the protein and sulphur atom of the cluster or sulphur atom of the cluster-liganding C133 leads to the general increase in the Orbach energy and may suggest that distances or angles between cluster atoms undergo modifications resulting in stronger spin–spin exchange coupling between  $\text{Fe}^{3+}$  and  $\text{Fe}^{2+}$  ions of the Fe–S cluster.

The efficiency of the Raman process ( $C_{\text{Ram}}$ ) generally increased exponentially with an increase in spectral anisotropy  $A$  (related to the spin–orbit coupling). Nevertheless, for some samples characterised by rather large spectral anisotropy, the expected increase of  $C_{\text{Ram}}$  was not observed. This lack of correlation can be interpreted as a reflection of changes in the rigidity of the protein that leads to modification of vibrational modes of

the Fe–S cluster, that overlays with the effects of changes in spin–orbit coupling. This suggests that upon formation or breaking of inter- or intramolecular hydrogen bonds and/or modification of interactions of the ISP-HD with other subunits of cytochrome  $bc_1$  the flexibility of the surroundings for the vibrational motions of the Fe–S cluster changes. It can be speculated that these changes contribute to the overall settings of the electrochemical properties of the cluster and may influence electron transfer between Fe–S and its redox partners during the reactions catalysed by cytochrome  $bc_1$ .

## Abbreviations

EPR	Electron paramagnetic resonance
Fe–S	Iron–sulphur
ISP	Iron–sulphur protein subunit
ISP-HD	Movable head domain of iron–sulphur protein subunit
tds	Tridecyl-stigmatellin
ato	Atovaquone
fam	Famoxadone
myx	Myxothiazol
ant	Antimycin
$E_m$	Redox midpoint potential
IR	Inversion recovery
CW	Continuous wave
$\theta_D$	Debye temperature
LMA	Levenberg–Marquardt algorithm

## Acknowledgements

This study was supported by The Wellcome Trust International Senior Research Fellowship (to A.O.) and the Polish Ministry of Science and Higher Education grant Iuventus Plus (to M.S.). We would like to thank Dr Monika Czapla for preparation of mutants of cytochrome  $bc_1$ .

## References

- 1 H. Beinert, Iron-Sulfur Proteins: Ancient Structures, Still Full of Surprises, *JBIC, J. Biol. Inorg. Chem.*, 2000, **5**(1), 2–15.
- 2 R. Cammack, F. MacMillan, Electron Magnetic Resonance of Iron-Sulfur Proteins in Electron-Transfer Chains: Resolving Complexity, in *Metals in Biology: applications of High-resolution EPR to Metalloenzymes, Biological Magnetic Resonance*, ed. G. Hanson and L. Berliner, 2010, vol. 29, pp. 11–44.
- 3 K. Brzóska, S. Męczyńska and M. Kruszewski, Iron-Sulfur Cluster Proteins: Electron Transfer and beyond, *Acta Biochim. Pol.*, 2006, **53**(4), 685–691.
- 4 L. Noodleman, T. Lovell, T. Liu, F. Himo and R. A. Torres, Insights into Properties and Energetics of Iron-Sulfur Proteins from Simple Clusters to Nitrogenase, *Curr. Opin. Chem. Biol.*, 2002, **6**(2), 259–273.



- 5 W. R. Hagen, EPR Spectroscopy of Iron-Sulfur Proteins, in *Advances in Inorganic Chemistry, Iron-Sulfur Proteins*, Academic Press, Inc., San Diego, 1992, pp. 165–222.
- 6 B. Guigliarelli and P. Bertrand, Application of EPR Spectroscopy to the Structural and Functional Study of Iron-Sulfur Proteins, *Adv. Inorg. Chem.*, 1999, **47**, 421–497.
- 7 M. Orio and J.-M. Mouesca, Variation of Average  $g$  Values and Effective Exchange Coupling Constants among  $[2\text{Fe}-2\text{S}]$  Clusters: A Density Functional Theory Study of the Impact of Localization (Trapping Forces) versus Delocalization (Double-Exchange) as Competing Factors, *Inorg. Chem.*, 2008, **47**(12), 5394–5416.
- 8 P. Bertrand, B. Guigliarelli, J.-P. Gayda, B. Peter and J. F. Gibson, A Ligand-Field Model to Describe a New Class of  $2\text{Fe}-2\text{S}$  Clusters in Proteins and Their Synthetic Analogues, *Biochim. Biophys. Acta, Protein Struct. Mol. Enzymol.*, 1985, **831**(2), 261–266.
- 9 W. R. Hagen, D. O. Hearsen, R. H. Sands and W. R. Dunham, A Statistical Theory for Powder EPR in Distributed Systems, *J. Magn. Reson.*, 1985, **61**(2), 220–232.
- 10 D. O. Hearshen, W. R. Hagen, R. H. Sands, H. J. Grande, H. L. Crespi, I. C. Gunsalus and W. R. Dunham, An Analysis of  $g$  Strain in the EPR of Two  $[2\text{Fe}-2\text{S}]$  Ferredoxins. Evidence for a Protein Rigidity Model, *J. Magn. Reson.*, 1986, **69**(3), 440–459.
- 11 A. Abragam and B. Bleaney, in *Electron Paramagnetic Resonance of Transition Ions*, ed. W. Marshall and D. H. Wilkinson, Clarendon Press, Oxford, 1970.
- 12 P. Bertrand, J. P. Gayda, J. A. Fee, D. Kuila and R. Cammack, Comparison of the Spin-Lattice Properties of the Two Classes of  $[2\text{Fe}-2\text{S}]$  Clusters in Proteins, *Biochim. Biophys. Acta*, 1987, **916**, 24–28.
- 13 J.-P. Gayda, P. Bertrand, A. Deville, C. More, G. Roger, J. F. Gibson and R. Cammack, Temperature Dependence of the Electronic Spin-Lattice Relaxation Time in a 2-Iron-2-Sulfur Protein, *Biochim. Biophys. Acta*, 1979, **581**, 15–26.
- 14 J.-P. Gayda, J. F. Gibson, R. Cammack, D. O. Hall and R. Mullinger, Spin Lattice Relaxation and Exchange Interaction in a 2-Iron, 2-Sulphur Protein, *Biochim. Biophys. Acta*, 1976, **434**, 154–163.
- 15 A. J. Fielding, S. Fox, G. L. Milihauser, M. Chattopadhyay, P. M. Kroneck, G. Fritz, G. Eaton and S. S. Eaton, Electron Spin Relaxation of copper(II) Complexes in Glassy Solution between 10 and 120 K, *J. Magn. Reson.*, 2006, **179**, 92–104.
- 16 H. Sato, V. Kathirvelu, A. J. Fielding, J. P. Blinco, A. S. Micallef, S. E. Bottle, S. S. Eaton and G. R. Eaton, Impact of Molecular Size on Electron Spin Relaxation Rates of Nitroxyl Radicals in Glassy Solvents between 100 and 300 K, *Mol. Phys.*, 2007, **105**, 2137–2151.
- 17 S. S. Eaton and G. R. Eaton, in *Biological Magnetic Resonance 19, Distance Measurement in Biological Systems by EPR*, ed. L. J. Berliner, S. S. Eaton and R. Gareth, Kluwer Academic Publishers, New York, 2002.
- 18 P. Bertrand, J. Gayda and K. K. Rao, Electron Spin-lattice Relaxation of the  $(4\text{Fe}-4\text{S})$  Ferredoxin from *B. Stearothermophilus*. Comparison with Other Iron Proteins, *J. Chem. Phys.*, 1982, **76**(10), 4715–4719.
- 19 E. A. Berry, M. Guergova-Kuras, L. Huang and A. R. Crofts, Structure and Function of Cytochrome  $bc$  Complexes, *Annu. Rev. Biochem.*, 2000, **69**, 1005–1075.
- 20 E. A. Berry, L.-S. Huang, L. K. Saechao, N. G. Pon, M. Valkova-Valchanova and F. Daldal, X-ray Structure of *Rhodobacter Capsulatus* Cytochrome  $bc_1$ : Comparison with Its Mitochondrial and Chloroplast Counterparts, *Photosynth. Res.*, 2004, **81**(3), 251–275.
- 21 M. Sarewicz and A. Osyczka, Electronic Connection Between the Quinone and Cytochrome  $c$  Redox Pools and Its Role in Regulation of Mitochondrial Electron Transport and Redox Signaling, *Physiol. Rev.*, 2015, **95**(1), 219–243.
- 22 Z. Zhang, L. Huang, V. M. Shulmeister, Y. I. Chi, K. K. Kim, L. W. Hung, A. R. Crofts, E. A. Berry and S. H. Kim, Electron Transfer by Domain Movement in Cytochrome  $bc_1$ , *Nature*, 1998, **392**(6677), 677–684.
- 23 E. Darrouzet, M. Valkova-Valchanova, C. C. Moser, P. L. Dutton and F. Daldal, Uncovering the  $[2\text{Fe}2\text{S}]$  Domain Movement in Cytochrome  $bc_1$  and Its Implications for Energy Conversion, *Proc. Natl. Acad. Sci. U. S. A.*, 2000, **97**(9), 4567–4572.
- 24 E. Darrouzet, C. C. Moser, P. L. Dutton and F. Daldal, Large Scale Domain Movement in Cytochrome  $bc_1$ : A New Device for Electron Transfer in Proteins, *Trends Biochem. Sci.*, 2001, **26**(7), 445–451.
- 25 J. W. Cooley, A. G. Roberts, M. K. Bowman, D. M. Kramer and F. Daldal, The Raised Midpoint Potential of the  $[2\text{Fe}2\text{S}]$  Cluster of Cytochrome  $bc_1$  Is Mediated by Both the  $Q_o$  Site Occupants and the Head Domain Position of the Fe-S Protein Subunit, *Biochemistry*, 2004, **43**(8), 2217–2227.
- 26 M. Sarewicz, M. Dutka, W. Froncisz and A. Osyczka, Magnetic Interactions Sense Changes in Distance between Heme  $b_L$  and the Iron-Sulfur Cluster in Cytochrome  $bc_1$ , *Biochemistry*, 2009, **48**, 5708–5720.
- 27 E. Darrouzet, M. Valkova-Valchanova and F. Daldal, Movement of the Iron-Sulfur Subunit beyond the  $ef$  Loop of Cytochrome  $b$  Is Required for Multiple Turnovers of the  $bc_1$  Complex but Not for Single Turnover  $Q_o$  Site Catalysis, *J. Biol. Chem.*, 2002, **277**(5), 3471–3476.
- 28 J. W. Cooley, T. Ohnishi and F. Daldal, Binding Dynamics at the Quinone Reduction ( $Q_i$ ) Site Influence the Equilibrium Interactions of the Iron Sulfur Protein and Hydroquinone Oxidation ( $Q_o$ ) Site of the Cytochrome  $bc_1$  Complex, *Biochemistry*, 2005, **44**(31), 10520–10532.
- 29 M. Sarewicz, A. Borek, E. Cieluch, M. Świerczek and A. Osyczka, Discrimination between Two Possible Reaction Sequences That Create Potential Risk of Generation of Deleterious Radicals by Cytochrome  $bc_1$ . Implications for the Mechanism of Superoxide Production, *Biochim. Biophys. Acta*, 2010, **1797**(11), 1820–1827.
- 30 F. Daldal, E. Davidson and S. Cheng, Isolation of the Structural Genes for the Rieske Fe-S Protein, Cytochrome  $b$  and Cytochrome  $c_1$  All Components of the Ubiquinol: Cytochrome  $c_2$  Oxidoreductase Complex of *Rhodospseudomonas Capsulata*, *J. Mol. Biol.*, 1987, **195**, 1–12.
- 31 E. Atta-Asafo-Adjei and F. Daldal, Size of the Amino Acid Side Chain at Position 158 of Cytochrome  $b$  is Critical for an



- Active Cytochrome  $bc_1$  complex and for photosynthetic growth of *Rhodobacter capsulatus*, *Proc. Natl. Acad. Sci. U. S. A.*, 1991, **88**(2), 492–496.
- 32 M. B. Valkova-Valchanova, A. S. Saribas, B. R. Gibney, P. L. Dutton and F. Daldal, Isolation and Characterization of a Two-Subunit Cytochrome  $b-c_1$  Subcomplex from *Rhodobacter Capsulatus* and Reconstitution of Its Ubihydroquinone Oxidation ( $Q_o$ ) Site with Purified Fe-S Protein Subunit, *Biochemistry*, 1998, **37**(10), 16242–16251.
  - 33 M. Czaplá, A. Borek, M. Sarewicz and A. Osyczka, Enzymatic Activities of Isolated Cytochrome  $bc_1$ -like Complexes Containing Fused Cytochrome  $b$  Subunits with Asymmetrically Inactivated Segments of Electron Transfer Chains, *Biochemistry*, 2012, **51**(4), 829–835.
  - 34 D. L. Williams-Smith, R. C. Bray, M. J. Barber, A. D. Tsopanakis and S. P. Vincent, Changes in Apparent pH on Freezing Aqueous Buffer Solutions and Their Relevance to Biochemical Electron-Paramagnetic-Resonance Spectroscopy, *Biochem. J.*, 1977, **167**, 593–600.
  - 35 R. Pietras, M. Sarewicz and A. Osyczka, Molecular Organization of Cytochrome  $c_2$  near the Binding Domain of Cytochrome  $bc_1$  Studied by Electron Spin-Lattice Relaxation Enhancement, *J. Phys. Chem. B*, 2014, **118**, 6634–6643.
  - 36 C. P. Lindsey and G. D. Patterson, Detailed Comparison of the Williams-Watts and Cole-Davidson Functions, *J. Chem. Phys.*, 1980, **73**(7), 3348–3357.
  - 37 W. Hagen, *Biomolecular EPR Spectroscopy*, CRC Press Taylor & Francis Group, Boca Raton, 2009.
  - 38 P. Thompson, D. E. Cox and J. B. Hastings, Rietveld Refinement of Debye–Scherrer Synchrotron X-ray Data from  $Al_2O_3$ , *J. Appl. Crystallogr.*, 1987, **20**(2), 79–83.
  - 39 T. Ida, M. Ando and H. Toraya, Extended Pseudo-Voigt Function for Approximating the Voigt Profile, *J. Appl. Crystallogr.*, 2000, **33**, 1311–1316.
  - 40 D. Wang and G. Hanson, A New Method for Simulating Randomly Oriented Powder Spectra in Magnetic Resonance: The Sydney Opera House (SOPHE) Method, *J. Magn. Reson., Ser. A*, 1995, **117**, 1–8.
  - 41 A. Ponti, Simulation of Magnetic Resonance Static Powder Lineshapes: A Quantitative Assessment of Spherical Codes, *J. Magn. Reson.*, 1999, **138**(2), 288–297.
  - 42 S. K. Hoffmann, W. Hiltzer, J. Goslar, M. M. Massa and R. Calvo, Electron Spin Relaxation in Pseudo-Jahn–Teller Low-Symmetry  $Cu(II)$  Complexes in  $Diaqua(l-Aspartate)Zn(II) \cdot H_2O$  Crystals, *J. Magn. Reson.*, 2001, **153**(1), 92–102.
  - 43 J. Nett, C. Hunte and B. L. Trumpower, Changes to the Length of the Flexible Linker Region of the Rieske Protein Impair the Interaction of Ubiquinol with the Cytochrome  $bc_1$  Complex, *Eur. J. Biochem.*, 2000, **267**, 5777–5782.
  - 44 A. Borek, M. Sarewicz and A. Osyczka, Movement of the Iron-Sulfur Head Domain of Cytochrome  $bc_1$  Transiently Opens the Catalytic  $Q_o$  Site for Reaction with Oxygen, *Biochemistry*, 2008, **47**(47), 12365–12370.
  - 45 T. Schroter, O. M. Hatzfeld, S. Gemeinhardt, M. Korn, T. Friedrich, B. Ludwig and T. A. Link, Mutational Analysis of Residues Forming Hydrogen Bonds in the Rieske [2Fe–2S] Cluster of the Cytochrome  $bc_1$  Complex in *Paracoccus Denitrificans*, *Eur. J. Biochem.*, 1998, **255**, 100–106.
  - 46 D. J. Kolling, J. S. Brunzelle, S. Lhee, A. R. Crofts and S. K. Nair, Atomic Resolution Structures of Rieske Iron-Sulfur Protein: Role of Hydrogen Bonds in Tuning the Redox Potential of Iron-Sulfur Clusters, *Structure*, 2007, **15**, 29–38.
  - 47 E. J. Leggate and J. Hirst, Roles of the Disulfide Bond and Adjacent Residues in Determining the Reduction Potentials and Stabilities of Respiratory-Type Rieske Clusters, *Biochemistry*, 2005, **44**(18), 7048–7058.
  - 48 M. Guergova-Kuras, R. Kuras, N. Ugulava, I. Hadad and A. R. Crofts, Specific Mutagenesis of the Rieske Iron-Sulfur Protein in *Rhodobacter Sphaeroides* Shows That Both the Thermodynamic Gradient and the pK of the Oxidized Form Determine the Rate of Quinol Oxidation by the  $bc_1$  Complex, *Biochemistry*, 2000, **39**(25), 7436–7444.
  - 49 E. Denke, T. Merbitz-Zahradnik, O. M. Hatzfeld, C. H. Snyder, T. A. Link and B. L. Trumpower, Alteration of the Midpoint Potential and Catalytic Activity of the Rieske Iron-Sulfur Protein by Changes of Amino Acids Forming Hydrogen Bonds to the Iron-Sulfur Cluster, *J. Biol. Chem.*, 1998, **273**(15), 9085–9093.
  - 50 V. P. Shinkarev, D. R. J. Kolling, T. J. Miller and A. R. Crofts, Modulation of the Midpoint Potential of the [2Fe–2S] Rieske Iron Sulfur Center by  $Q_o$  Occupants in the  $bc_1$  Complex, *Biochemistry*, 2002, **41**(48), 14372–14382.
  - 51 A. M. Kuznetsov, E. M. Zueva, A. N. Masliy and L. I. Krishtalik, Redox Potential of the Rieske Iron-sulfur Protein: Quantum-chemical and Electrostatic Study, *Biochim. Biophys. Acta*, 2010, **1797**(3), 347–359.
  - 52 L. Esser, B. Quinn, Y.-F. Li, M. Zhang, M. Elberry, L. Yu, C.-A. Yu and D. Xia, Crystallographic Studies of Quinol Oxidation Site Inhibitors: A Modified Classification of Inhibitors for the Cytochrome  $bc_1$  Complex, *J. Mol. Biol.*, 2004, **341**(1), 281–302.
  - 53 G. Von Jagow and T. A. Link, Use of Specific Inhibitors on the Mitochondrial  $bc_1$  Complex, *Methods Enzymol.*, 1986, **126**, 253–271.
  - 54 E. A. Berry and L.-S. Huang, Conformationally Linked Interaction in the Cytochrome  $bc_1$  Complex between Inhibitors of the  $Q_o$  Site and the Rieske Iron-Sulfur Protein, *Biochim. Biophys. Acta*, 2011, **1807**(10), 1349–1363.
  - 55 J. J. Kessl, B. B. Lange, T. Merbitz-Zahradnik, K. Zwicker, P. Hill, B. Meunier, H. Palsdottir, C. Hunte, S. Meshnick and B. L. Trumpower, Molecular Basis for Atovaquone Binding to the Cytochrome  $bc_1$  Complex, *J. Biol. Chem.*, 2003, **278**(33), 31312–31318.
  - 56 S. K. Nayak, S. B. Mallik, S. P. Kanaujia, K. Sekar, K. R. Ranganathan, V. Ananthakrishni, G. Jeyaraman, S. S. Saralaya, K. S. Rao and K. Shridhara, *et al.* Crystal Structures and Binding Studies of Atovaquone and Its Derivatives with Cytochrome  $bc_1$ : A Molecular Basis for Drug Design, *CrystEngComm*, 2013, **15**(24), 4871–4884.
  - 57 V. Barton, N. Fisher, G. A. Biagini, S. A. Ward and P. M. O'Neill, Inhibiting *Plasmodium* Cytochrome  $bc_1$ : A Complex Issue, *Curr. Opin. Chem. Biol.*, 2010, **14**(4), 440–446.



- 58 X. Gao, X. Wen, C. C.-A. Yu, L. Esser, S. Tsao, B. Quinn, L. Zhang, L. Yu and D. Xia, The Crystal Structure of Mitochondrial Cytochrome  $bc_1$  in Complex with Famoxadone: The Role of Aromatic-Aromatic Interaction in Inhibition, *Biochemistry*, 2002, **41**(39), 11692–11702.
- 59 F. L. Muller, A. G. Roberts, M. K. Bowman and D. M. Kramer, Architecture of the  $Q_o$  Site of the Cytochrome  $bc_1$  Complex Probed by Superoxide Production, *Biochemistry*, 2003, **42**(21), 6493–6499.
- 60 I. Bertini, S. Ciurli, C. Luchinat, V. G. Capponi, V. B. Pichat and V. Distribution, The Electronic Structure of FeS Centers in Proteins and Models a Contribution to the Understanding of Their Electron Transfer Properties, *Struct. Bonding*, 1995, **83**, 1–53.
- 61 S. A. Fiethen, V. Staemmler, N. N. Nair, J. Ribas-Arino, E. Schreiner and D. Marx, Revealing the Magnetostructural Dynamics of  $[2Fe-2S]$  Ferredoxins from Reduced-Dimensionality Analysis of Antiferromagnetic Exchange Coupling Fluctuations, *J. Phys. Chem. B*, 2010, **114**(35), 11612–11619.
- 62 Y. Zhou, B. E. Bowler, G. R. Eaton and S. S. Eaton, Electron Spin Lattice Relaxation Rates for  $S = 1/2$  Molecular Species in Glassy Matrices or Magnetically Dilute Solids at Temperatures between 10 and 300 K, *J. Magn. Reson.*, 1999, **174**, 165–174.
- 63 R. J. Usselman, A. J. Fielding, F. E. Frerman, N. J. Watmough, G. R. Eaton, S. S. Eaton and M. Simkovic, Impact of Mutations on the Midpoint Potential of the  $[4Fe-4S]^{+1,+2}$  Cluster and on Catalytic Activity in Electron Transfer Flavoprotein-Ubiquinone Oxidoreductase (ETF-QO), *Biochemistry*, 2008, **47**(1), 92–100.
- 64 S. Iwata, J. W. Lee, K. Okada, J. K. Lee, M. Iwata, B. Rasmussen, T. A. Link, S. Ramaswamy and B. K. Jap, Complete Structure of the 11-Subunit Bovine Mitochondrial Cytochrome  $bc_1$  Complex, *Science*, 1998, **281**, 64–71.

